AIP Advances

Deagglomeration of nanoparticle clusters in a "cavitation on chip" device

Cite as: AIP Advances **10**, 115204 (2020); https://doi.org/10.1063/5.0029070
Submitted: 09 September 2020 . Accepted: 16 October 2020 . Published Online: 03 November 2020

Moein Talebian Gevari, Soroush Niazi, Mehrdad Karimzadehkhouei, Kursat Sendur, M. Pinar Menguc, Morteza Ghorbani, and Ali Koşar

COLLECTIONS

Paper published as part of the special topic on Chemical Physics, Energy, Fluids and Plasmas, Materials Science and Mathematical Physics

View Online Export Citation CrossMark

ARTICLES YOU MAY BE INTERESTED IN

Energy harvesting with micro scale hydrodynamic cavitation-thermoelectric generation coupling
AIP Advances **9**, 105012 (2019); https://doi.org/10.1063/1.5115336

Effect of intensified cavitation using poly(vinyl alcohol) microbubbles on spray atomization characteristics in microscale
AIP Advances **10**, 025318 (2020); https://doi.org/10.1063/1.5142607

Photovoltaic properties of all-inorganic lead-free perovskite Cs_2PdBr_6: A first-principles study
AIP Advances **10**, 115203 (2020); https://doi.org/10.1063/5.0029738

AIP Advances
Fluids and Plasmas Collection
READ NOW

AIP Publishing

© 2020 Author(s).

Deagglomeration of nanoparticle clusters in a "cavitation on chip" device

Cite as: AIP Advances 10, 115204 (2020); doi: 10.1063/5.0029070
Submitted: 9 September 2020 • Accepted: 16 October 2020 •
Published Online: 3 November 2020

View Online Export Citation CrossMark

Moein Talebian Gevari,[1,2] Soroush Niazi,[1,2] Mehrdad Karimzadehkhouei,[3] Kursat Sendur,[2,4] M. Pinar Menguc,[5] Morteza Ghorbani,[1,4,6,a)] and Ali Koşar[1,2,4,a)]

AFFILIATIONS

[1]Sabanci University Nanotechnology Research and Application Center, Tuzla, 34956 Istanbul, Turkey
[2]Faculty of Engineering and Natural Sciences, Sabanci University, Tuzla, 34956 Istanbul, Turkey
[3]Department of Mechanical Engineering, Koç University, Rumelifeneri Yolu, Sariyer, 34450 Istanbul, Turkey
[4]Center of Excellence for Functional Surfaces and Interfaces for Nano-Diagnostics (EFSUN), Sabanci University, Orhanli, Tuzla, 34956 Istanbul, Turkey
[5]Center for Energy, Environment and Economy, Ozyegin University, Istanbul 34794, Turkey
[6]Department of Biomedical Engineering and Health Systems, KTH Royal Institute of Technology, SE-141 57 Stockholm, Sweden

[a)]**Authors to whom correspondence should be addressed:** morteza@sabanciuniv.edu and kosara@sabanciuniv.edu

ABSTRACT

Due to the potential of significant energy release in cavitating flows, early cavitation inception and intensification of cavitating flows are of great importance. To use this potential, we investigated the deagglomeration of nanoparticle clusters with the implementation of hydrodynamic cavitation in a microfluidic device. For this purpose, a microfluidic device with a micro-orifice geometry was designed and fabricated using standard microfabrication processes. The system was tested with distilled water in the assembled experimental setup. The flow patterns were characterized using the cavitation number and inlet pressure. Titania nanoparticles were utilized to prepare nanoparticle suspensions. The suspensions were heated to allow agglomeration of nanoparticles. The system was operated with the new working fluid (nanoparticle clusters) at different inlet pressures. After characterizing flow patterns, the flow patterns were compared with those of pure water. The deagglomeration effects of hydrodynamic cavitation on nanoparticle clusters showed the possibility to apply this method for the stabilization of nanoparticles, which paves way to the implementation of nanoparticle suspensions to thermal fluid systems for increased energy efficiency as well as to drug delivery. Our results also indicate that the presence of nanoparticles in the working fluid enhanced cavitation intensity due to the increase in the number of heterogeneous nucleation sites.

© 2020 Author(s). All article content, except where otherwise noted, is licensed under a Creative Commons Attribution (CC BY) license (http://creativecommons.org/licenses/by/4.0/). https://doi.org/10.1063/5.0029070

I. INTRODUCTION

Cavitation has been known as a destructive phenomenon for a long time in the field of fluid mechanics, especially in turbomachinery. Cavitation occurs as a consequence of an abrupt pressure drop in fluidic systems, where the local pressure of the working fluid is reduced to a level below the saturation vapor pressure. Although many research efforts were made to overcome this issue in turbomachinery,[1] many studies also focused on utilizing the massive amount of energy released by the collapse of cavitation bubbles in the food industry,[2,3] heat transfer,[4,5] biomedical devices,[6] energy harvesting,[7,8] water treatment,[9] biodiesel production,[10] and bacteria disinfection.[11]

With the emergence of microfluidics, hydrodynamic cavitation has been considered as an important alternative to ultrasonic cavitation. Due to the higher surface area to volume ratio in microfluidics, the bubble collapse energy could be more efficiently exploited in a desired application. In addition, a hydrodynamic cavitation on chip platform can be regarded as a passive system. Therefore, the energy efficiency will be higher than an ultrasonic cavitation setup.

Hydrodynamic cavitation occurs when there is a flow restrictive element along the fluid path such as an orifice. Due to the

huge potential of energy release[12] in cavitating flows, early cavitation inception and intensification of cavitating flows are of great significance, which can be achieved by optimizing the channel geometry and/or changing the working fluid. There is increasing interest in this research field. As an example, Šarc *et al.*[13] studied the effect of geometry on cavitation. Im *et al.*[14] emphasized on the importance of nozzle geometry in generating cavitation flows. Ghorbani *et al.*[15] implemented surface roughness in microfluidic devices and concluded that devices with roughness elements provided earlier cavitation inception. In their study, roughness was applied using an optimized deep reactive ion etching (DRIE) system, while the size of peak-to-peak surface roughness was about 5 μm. In another study, the surface of the microfluidic device was modified with silica nanoparticles (CNF-stabilized PFC5), which facilitated cavitation inception.[16] Besides surface roughness, sidewall roughness was applied due to the fact that heterogeneous nucleation occurred on the orifice wall in the presence of crevices.[15] Thus, implementing the roughness at the beginning of the orifice wall resulted in cavitation inception at lower inlet pressures.[17] Gevari *et al.*[18] optimized the sidewall roughness elements in terms of length and height for achieving a more efficient microfluidic device in terms of generating cavitating flows.

The working fluid is the other important parameter affecting cavitation intensification and has also been recently studied. For instance, Mossaz *et al.*[19] studied the effect of isopropanol and water mixture as the working fluid. Adding isopropanol to water caused cavitation inception in the laminar flow regime instead of the turbulent flow regime. Mishra and Peles[20] compared the results of water, ethanol, and refrigerants in their cavitation experimental setup and concluded that lower surface tension fluid led to the easier generation of cavitation bubbles in micro-scale. Suspensions of poly (vinyl alcohol) (PVA) microbubbles in water were also studied in microfluidic devices[21] and transparent cylindrical nozzles.[22] Accordingly, PVA suspensions resulted in more intensified cavitating flows than the reference fluids. Water and perfluoropentane (PFC5) droplet-water suspensions were tested in a micro-orifice for obtaining their performances in energy harvesting.[7] The results showed that cavitation inception and supercavitation conditions occurred at lower inlet pressures, and the cavitation intensity was higher in perfluoropentane (PFC5) droplet-water suspensions.

Nanoparticle suspensions include a base fluid with nanoparticles with sizes less than 100 nm. They have many applications in drug and gene deliveries,[23] microbial fuel cells (MFCs),[24] biomedical applications,[25] pollution filtration,[26] cancer therapy,[27] thermal systems,[28] heat transfer enhancement,[29] and energy storage.[30] Based on their applications, various types of nanoparticles can be utilized. They have attracted the attention of many researchers in many fields due to the Brownian motion, high thermal conductivity, and high surface to volume ratio of nanoparticles.[31] While nanoparticle suspensions have many superior advantages, they have a major issue in their implementation. Nanoparticles become gradually agglomerated with time and absorption of heat, which causes instability and results in sedimentation. As a result, stability studies on nanoparticles have gained significant attention.[32,33] The most commonly used solution for this issue is the use of surfactants.[34] However, this approach alters thermophysical properties, and it might generate foam and contaminate the operating system in the long run. Moreover, the surfactants might lose their functionality at high temperatures.[35] A surfactant-free technique of enhancing the stability of nanoparticle suspensions is nanoparticle surface modification such as grafting silanes directly to the surface of silica nanoparticles for synthesis of functionalized silica (SiO_2). However, this approach is also challenging since it requires expensive fabrication processes.[36]

The interaction of cavitation and nanoparticle suspensions is an attractive research area since cavitation offers direct and indirect thermal and energy applications,[37] and nanoparticle suspensions are also being employed in many applications including thermal systems. In this article, the effect of hydrodynamic cavitation on improving the stability of agglomerated titania nanoparticle suspensions was investigated in a microfluidic "cavitation on chip" device. The concept of the proposed technique was proven in a proof of concept study by the authors,[38,39] using a microtube with an orifice in an open-loop system. In this study, the mentioned concept is implemented to a microfluidic device. The presented concept within a microfluidic device will pave way to the design and development of devices for increasing the stability and reusability of nanoparticle suspensions as well as for increasing the energy efficiency in thermal systems and processes.

II. MATERIAL AND METHODS

A. Experimental setup

The experimental hydrodynamic cavitation setup shown in Fig. 1 includes a high-pressure nitrogen tank (Linde Gas, Gebze, Kocaeli, Turkey) to push the working fluid into the system. The working fluids, commercial titania nanoparticle-water suspensions with a weight fraction of 0.05% and pure water, are separately kept inside the fluid container (Swagelok, Erbusco BS, Italy), which is equipped with a pressure gauge (Omega) to measure the pressures at the outlet of the fluid container. Stainless steel tubing and appropriate Swagelok fittings are used to guide the working fluids to the chip holder, where the microfluidic device was installed. The chip holder consists of one inlet, two outlets, and three pressure ports, which allow measurement of static pressure at three different locations of the microfluidic device. The microfluidic device, on the other hand, houses a high-pressure resistant micro-orifice etched on a silicon substrate. The widths of the inlet and extension of the device are 900 μm, and the width of the micro-orifice is 152 μm. The total length of the microfluidic device is 6 mm, which is divided equally into three regions along the device. To enhance the cavitation intensity, sidewall roughness elements are added to the orifice's wall with a height of 1% of the width of the micro-orifice along the entire length. The microfluidic device is sandwiched to the chip holder by two Plexiglass slabs using screws and bolts. Silicon O-rings are used between the microfluidic device and the chip holder to prevent any leakage from the device. A proper light source provides necessary illumination for the high-speed camera (Phantom v310, Vision RESEARCH) so that flow patterns can be clearly recognized during the experiments. Dynamic light scattering (DLS, Zetasizer Nano ZS, Malvern) is utilized to measure the average hydrodynamic diameter of nanoparticles before and after the experiments. More details are available in the previous article by the authors.[38]

© Author(s) 2020

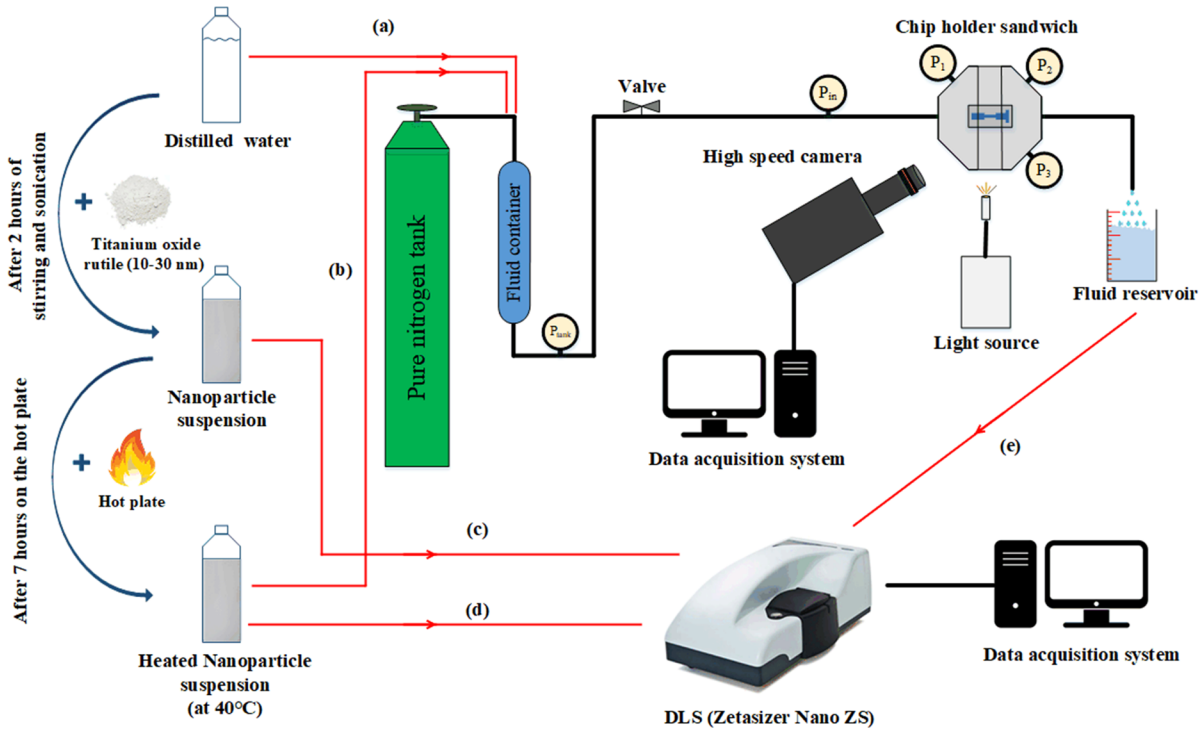


FIG. 1. Experimental setup and summary of the experimental procedure (nanoparticle suspension preparation, hydrodynamic cavitation setup, and DLS measurements): (a) the cavitation phenomena are characterized using distilled (DI) water, (b) the heated nanoparticle suspension is used as the working fluid, and the flow patterns are inspected, (c) the hydraulic diameter of the nanoparticle suspension is measured using a DLS device, (d) the hydraulic diameter of the heated nanoparticle suspension is measured using the DLS device, and (e) the exiting nanoparticle suspension after being exposed to cavitating flow is used for DLS measurements.

B. Microfluidic device geometry and fabrication

The fabricated microfluidic device is capable of withstanding pressures up to about 7.2 MPa.[16] The fabrication process flow includes five main steps. A double side polished ⟨100⟩ silicon wafer was used. A 500 nm thick layer of silicon dioxide was deposited on both sides of the silicon wafer using plasma enhanced chemical vapor deposition (PECVD). The pattern of the microchannel was transferred on the substrate by photolithography. The patterns of the inlet, outlets, and pressure ports were transferred on the substrate as second photolithography in this fabrication. A 200 μm deep etching of the silicon substrate was achieved by deep reactive ion etching. After the resist strip, a further 50 μm deep dry etching of silicon was performed to form both the holes and the microchannel pattern on the substrate. The masking layer of silicon dioxide was then removed by wet etching in a buffered oxide etchant (BOE). The substrate was then cleaned using the Piranha cleaning process and was anodically bonded to Borofloat 33 glass. The details of the fabrication process flow can be found in a recent study by the authors.[18] The configuration of the fabricated microfluidic device is shown in Fig. 2 along with the geometrical dimensions in Table I.

C. Nanoparticle suspension (nanofluid) preparation

Spherical commercial titanium oxide powder rutile (Ionic Liquids Technologies, IoLiTec GmbH, Germany) with a particle mean diameter of 10 nm–30 nm was used to prepare the suspension with a weight ratio of 0.05 wt. % in distilled (DI) water (as the base fluid). More characterization results are available in the previous article by the authors.[38] The suspension was stirred and sonicated for 2 h to ensure that a stable fluid with a weight ratio of 0.05%

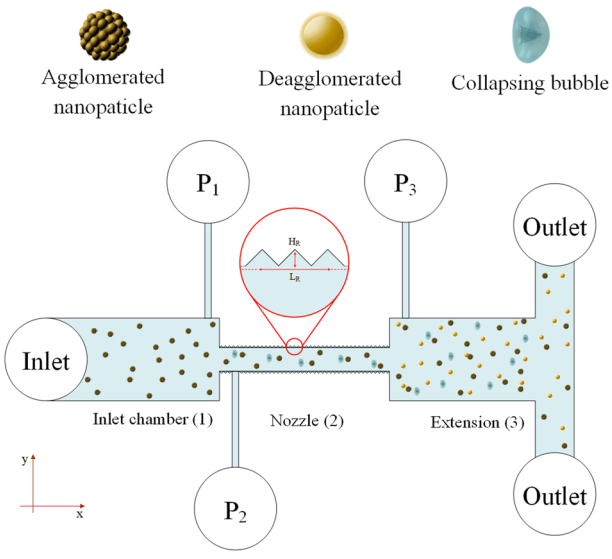


FIG. 2. Schematic of the fabricated microfluidic device.

© Author(s) 2020

TABLE I. Dimensions of the microfluidic device.

	Length (μm)	Width (μm)
Total microfluidic device	6000	[a]50
Inlet chamber	2000	900
Nozzle	2000	152
Extension	2000	900
Roughness elements	2000	1.5

[a]This value is the depth of the microfluidic device.

can be obtained. Dynamic light scattering (DLS) was used to measure the hydrodynamic diameter of particles in the suspension. The refractive index of TiO_2 rutile powder was 2.6142.[40] DLS measurements were performed three times, and in each run, the fluid was tested for at least 15 times. The reported z-average shows the mean hydrodynamic diameter of the particles, which is 255 nm. Then, the sample was heated up to 40 °C on a hot plate and was simultaneously stirred for 7 h until nanoparticle agglomeration happened. DLS measurements after this process led to a mean hydrodynamic diameter of 1281 nm. The agglomerated particles were used to investigate the deagglomeration of nanoparticles via hydrodynamic cavitation.

III. RESULTS AND DISCUSSION

A. Homogeneous and heterogeneous nucleation

Both cavitation inception and cavitating flow patterns are dependent on different parameters. In an ideal working fluid being free of contamination and/or dissolved gases, nucleation of the bubbles appears in two types: homogeneous and heterogeneous. Homogeneous nucleation occurs in the bulk of the fluid far from the walls, or in other words, it occurs far from the solid boundary with the liquid. From the microscopic perspective, the molecules with higher kinetic energy due to radiation, thermal shocks, or aggressive collision with other molecules are susceptible to phase change as being surrounded by a low-pressure region.[41] It should be noted that studying pure homogeneous nucleation is practically complicated since a pure working fluid is hard to obtain. Heterogeneous nucleation, on the other hand, happens on the nucleation sites on the solid boundary. The presence of surface roughness on the wall in contact with the working fluid facilitates the earlier inception of cavitating flows.

From the theoretical perspective, when the static pressure drops to a level below the saturated vapor pressure of the working fluid in a fluidic system, homogeneous nucleation happens. However, there are different parameters, whose presence (in some cases whose absence) can adversely affect cavitation inception. For instance, the dissolved gas in the working fluid tends to leave the bulk of the fluid under a static pressure drop in the form of bubbles. The presence of impurities alters the thermophysical properties of the working fluid such as density, vapor saturation pressure, and surface tension. Besides, the presence of solid contamination even in submicron size triggers heterogeneous nucleation and may be misinterpreted as homogeneous nucleation. Surface roughness, on the other hand, can also lower the inlet pressure necessary for generating cavitating flows.[41]

The most commonly used parameter to characterize cavitating flows is the dimensionless cavitation number expressed as[17]

$$\sigma = \frac{(P - P_{vap})}{0.5\rho V^2}, \tag{1}$$

where P is the inlet pressure, P_{vap} is the vapor saturation pressure, which is 2.33 kPa for water at room temperature, ρ is the density of the fluid, and V is the velocity of the working fluid (inside the microchannel in this study). A smaller value of the cavitation number suggests more intense cavitation.

In this study, impurities as titania nanoparticles were added to the working fluid to facilitate and intensify hydrodynamic cavitation. For this purpose, cavitating flows were characterized with filtered DI (de-ionized) water in the fabricated microfluidic device and were then compared to those with 0.05 wt. % titania nanoparticle suspensions. The reference velocity is calculated at the beginning of the nozzle area from flowrate measurements during the experiments. Since the concentration of the nanoparticles in the base fluid is rather low, the changes in the vapor saturation pressure and density of the fluid are neglected.

B. Theoretical energy analysis of cavitating flow

The generated cavitation bubbles carry a significant amount of potential energy released upon collapse. The released energy is converted to heat, noise, vibration, and shock waves. Previous studies show that the local high pressure and temperature spots in acoustic cavitation could have values up to 500 atm and 5000 K, respectively,[12] while the bubble content, i.e., dissolved gas content and surrounding temperature, strongly affects the collapse mechanism in hydrodynamic cavitation.

The results of our recent study[7] reveal that the average size of the generated bubbles in the tested microfluidic device was 3.5 μm in diameter. The bubble number density in a control volume is estimated as[7,42]

$$n = \frac{\alpha}{\frac{4}{3}\pi R^3}, \tag{2}$$

where α is the volume fraction of the vapor phase and R is the average bubble radius of the bubbles. Considering the supercavitation condition, where the cavitation intensity is high, and α theoretically approaches one, the bubble number density for this geometry spans around 44×10^6 mm^{-3}. Thus, the number of bubbles present within a small volume of the microfluidic device (in the micro-orifice section) is substantially high (≈669 000), which implies a significant energy release upon collapse. On the other hand, the potential energy of each cavitation bubble is calculated as[43]

$$E_{pot} = \frac{4}{3}\pi R^3 (P_{stat} - P_{vap}), \tag{3}$$

where P_{stat} is the static pressure of the system and P_{vap} is the vapor saturation pressure of the working fluid. Multiplying the potential energy with the number of bubbles gives an estimation of the energy released upon collapse. Considering the above-mentioned values, the potential energy inside the nozzle region is calculated as 1.46 μJ, which represents a considerable amount of energy released within a small confinement ($152 \times 2000 \times 50$ μm^3).

© Author(s) 2020

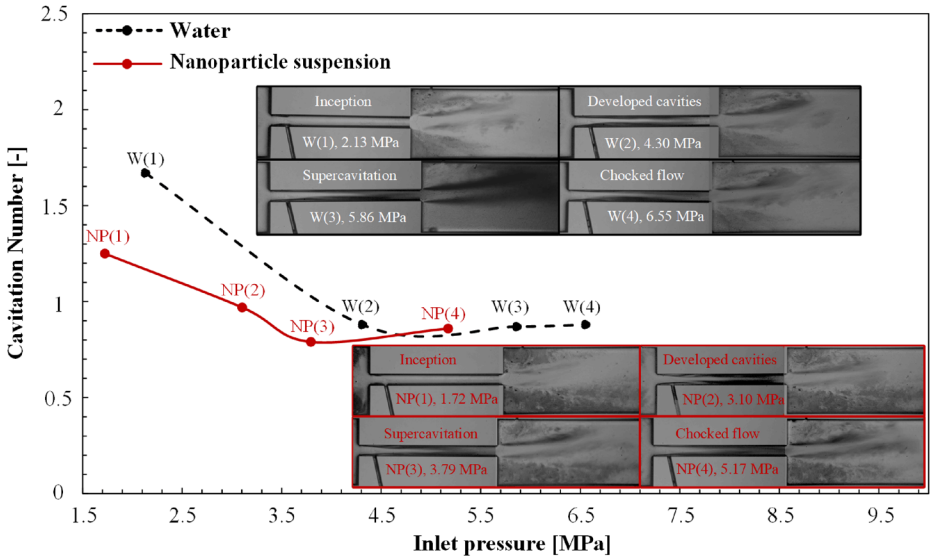


FIG. 3. Flow patterns of the cavitating flow in the microfluidic device at different inlet pressures and cavitation numbers (W = water and NP = nanoparticle suspension).

C. Effects of nanoparticles on nucleation

In the first set experiments, filtered DI water was used as the working fluid, and experiments were conducted at different inlet pressures with a focus on the inception of cavitating flows. According to the results, cavitation inception occurs at 2.13 MPa corresponding to the cavitation number of 1.67, while supercavitation is observed at 5.86 MPa corresponding to the cavitation number of 0.87. In the second set of experiments, nanoparticle suspensions were tested. Both the inception and development of the cavitating flows occur earlier in this case. In this case, the inception of the cavitation happens at 1.72 MPa, which is less than the case with DI water. Figure 3 shows the cavitation number and flow patterns for both cases at different inlet pressures.

As shown in Fig. 3, the development of cavitating flow is faster in the case of nanoparticle suspension than the case with DI water. According to Eq. (1), the cavitation number decreases with inlet pressure due to the square of velocity in the denominator. The decreasing trend in the cavitation number shown in Fig. 3 prevails until the third point. Beyond the supercavitation condition, the flow rate is saturated so that the velocity of the fluid does not change significantly with the inlet pressure, which raises the cavitation number. As a result, the cavitation number starts to increase. The same trends can be seen in both cases shown in Fig. 3. Due to the difference in cavitation numbers at the same inlet pressure, it is evident that the intensity of cavitating flow is higher for the case of nanoparticle suspension. The cavitation number under the supercavitation condition for this case is 0.79, while this number is around 0.7 for the case of water. The same trend is seen in other flow patterns. The cavitation number at inception is 1.67 for the case of water, while it is 1.25 for the case of the nanoparticle conditions (at lower inlet pressure), which implies more intense cavitating flow under the same condition. This finding is the motivation for using nanoparticle suspensions for intensifying microscale hydrodynamic cavitation.

The turbulent effects, as demonstrated in Fig. 3 and also reported in our previous studies, lead to high intensity cavitating flows because of both the pressure recovery at the extension and the local high velocity vortices in the microfluidic device. The high efficiency of this device is linked to these multiple physical phenomena at high pressure and velocities.

D. Deagglomeration effect of cavitating flow

As mentioned before, cavitating flows have deagglomeration effects on nanoparticle clusters. The results from DLS measurements show that the average hydrodynamic diameter of the nanoparticles was initially 255 nm before heating, whereas the average hydrodynamic diameter reached 1281 nm after heating and stirring. The prepared suspension was fed to the system, and the tested samples were taken for DLS measurements to demonstrate the increase in the stability of nanoparticles. The results of the DLS measurements are shown in Fig. 4.

As can be observed from these results, substantial deagglomeration of heated nanoparticle clusters can be achieved with the present approach. The exposed nanoparticle suspension has an average size of 164 nm at high pressure, which is even smaller than the diameter of the original suspension and serves as proof of increased nanoparticle stability. While the pressure corresponding to the inception for the case of nanoparticle suspension is 1.72 MPa, 84% size reduction happens at a pressure (2 MPa) close to the inception pressure. This emphasizes on the effectiveness of cavitation even at its inception. At cavitation inception, in addition to bubble collapse, the tensile strength of the working fluid also changes dramatically so that bubbles can form. The change in tensile strength and the work carried out by the gas phase on the surrounding molecules to form the bubble offer additional effects on the deagglomeration of nanoparticle clusters. It is worthwhile to note that the nanoparticle clusters achieve a mean diameter of 255 nm after a 2 h sonication. However, after their agglomeration due to heating, the reduction in their mean diameter happens in a few microseconds when exposed to cavitation bubble collapse. This serves as the proof of concept of the proposed

© Author(s) 2020

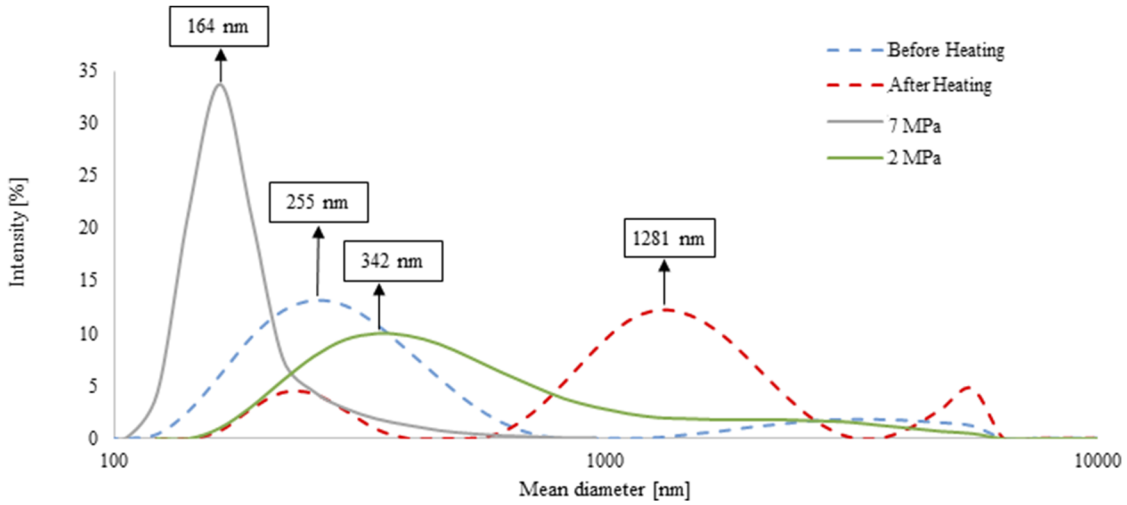


FIG. 4. DLS measurement results of the nanoparticles before heating, after heating, and after being exposed to cavitating flows at 2 MPa and 7 MPa.

method, which relies on hydrodynamic cavitation resulting in the generation of bubbles at the nucleation site anywhere in the fluid and especially on the nanoparticle clusters. However, in sonication, the bubbles are generated close to the sonication probes and are not necessarily close to all the dispersed nanoparticle clusters in the base fluid.

To validate the effect of bubble collapse on the nanoparticle cluster deagglomeration, the impact pressure of the bubble collapse can be estimated. The impact pressure of the hydrodynamic cavitation bubble collapse is expressed as[38]

$$P_{imp} = \frac{\rho_l c_l v_{jet}}{1 + (\rho_l c_l / \rho_s c_s)}, \tag{4}$$

where ρ_l and c_l are the density and sound speed in the liquid phase, respectively, and ρ_s and c_s are the corresponding values for the solid phase. v_{jet}, on the other hand, is the velocity of the liquid jet in the nozzle area. The sound speed in the water at 20 °C is 1531 m/s, while this value for the titanium dioxide is significantly higher with respect to the high Young modulus of titanium dioxide ($c_s = \sqrt{E_s/\rho_s}$), which is 250 GPa. As a result, the denominator in Eq. (4) can be approximated as 1, and the equation is written as

$$P_{imp} = \rho_l c_l v_{jet}. \tag{5}$$

The impact pressure as a function of the cavitation number and Reynolds number ($Re = \rho v D_h/\mu$) at the nozzle (restrictive element) is shown in Fig. 5.

As can be seen, the minimum impact pressure of cavitating flow is 80 MPa, and it increases up to 175 MPa, which illustrates the amount of energy release on the agglomerated nanoparticles. The modulus of rupture in titanium dioxide (rutile) is 140 MPa. Thus, it is evident that the impact pressure is in the vicinity of this modulus, which proves that the deagglomeration is due to the bubble collapse. On the other hand, one important feature of the present microfluidic devices lies in its resistance to high pressures. The high-pressure system leads to high velocities and Reynolds number. As can be seen in Fig. 5, the flow is turbulent as the Reynolds number varies between 9000 and 20 000. The high intensity turbulent flow along with the design of the microfluidic devices with an efficient pressure recovery at the extension leads to numerous local vortices. The velocity at the center of vortices is significantly higher than the average velocity in the device. Hence, cavitation could occur in these regions as well. In other words, this study takes advantage of this turbulent flow physics for the deagglomeration of nanoparticle clusters.

The experiments were repeated for the second time. The mean diameter of the nanoparticles was measured as 1051 nm after heating. The sample was tested at inlet pressures of 2.06 MPa, 4.48 MPa, and 6.2 MPa corresponding to the inception of cavitation, developed cavitation, and supercavitation flow patterns. The experimental results from the second set of experiments are in close agreement with those of the first set.

The reduction ratio as a function of the cavitation number is displayed in Fig. 6. The relationship between the reduction ratio and the cavitation number has a similar trend with our previous study in an open-loop system.[38]

As can be seen, in the first set of experiments, a reduction ratio of over 100% is achieved, which implies that the final size is lower than the initial size of the cluster, proving the effectiveness of this method and suggesting that this method can be implemented in thermal-fluid systems for energy efficiency. A second-degree polynomial curve fit successfully represents the data shown in Fig. 6 for both sets of the experiments.

The method presented in this study offers interesting real life energy applications for use of nanoparticle suspensions in thermal management, refrigeration, drug delivery, energy saving, and heat sink design while maintaining their stability. This method does not involve any use of extensive surfactants or surface modifiers, which might alter thermophysical properties of nanoparticle suspensions, adversely influencing their performance and biocompatibility, and

© Author(s) 2020

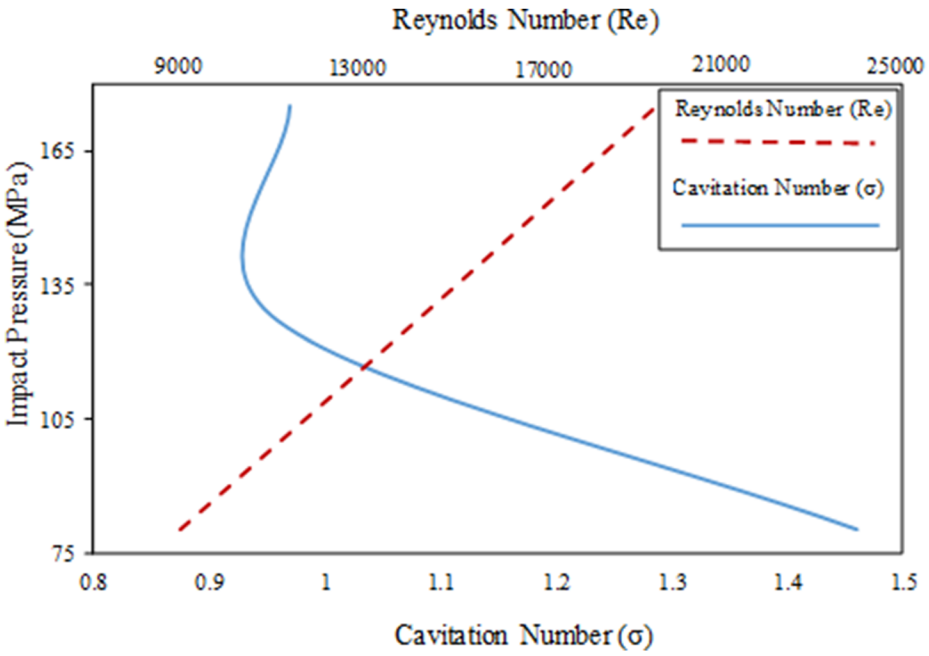


FIG. 5. Impact pressure as a function the Reynolds number and cavitation number.

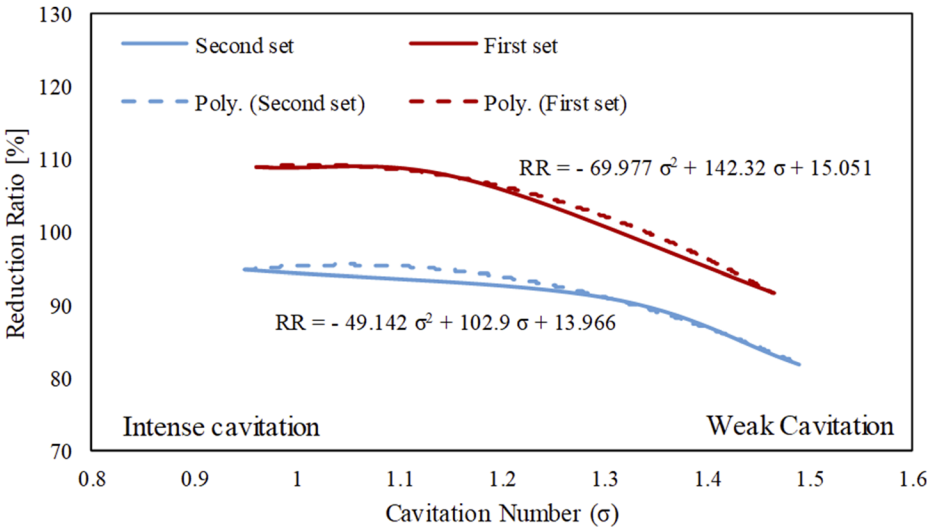


FIG. 6. Nanoparticle hydrodynamic diameter reduction ratio as a function of cavitation number.

limit their effectiveness. This approach is also more economical since no expensive chemicals are included. The integration of flow restrictive elements can be easily accomplished in terms of a new flow component, where flow restrictive elements can be formed by standard microfabrication tools and techniques within the flow component, which can be added to any energy system with standard fittings. Additional pressure and temperature sensors and a DLS system can also be integrated to this flow component so that real-time temperature, pressure, and nanoparticle hydrodynamic size measurements can be made.

IV. CONCLUSIONS

In this study, the effect of nanoparticle presence on cavitating flow patterns was investigated in a "cavitation on a chip" device. A significant enhancement in cavitation intensity and earlier cavitation inception was obtained with the use of nanoparticle suspensions. The experimental results and their trends match well with the existing theory. Besides, suspensions with agglomerated nanoparticles, which were prepared by heating, were tested under cavitating flow conditions. The effect of cavitating flows on the

© Author(s) 2020

stability and deagglomeration of the nanoparticle suspensions was thus investigated. The results exhibited an outstanding performance of deagglomeration. Our results indicate that the average nanoparticle hydrodynamic diameter decreased from 1281 nm to 342 nm and 164 nm at inlet pressures of 2 MPa and 7 MPa, respectively. Even inlet pressures close to pressures corresponding to cavitation inception resulted in significant deagglomeration, which was explained by the tensile strength change in the working fluids in addition to the energy released upon bubble collapse.

The presented microfluidic device offers turbulent flows in the fluid flow path, which lead to the presence of several high velocity vortices and low-pressure nodes. The combination of turbulence with cavitating flows and the change in fluid tensile strength could result in a high efficiency device, which achieves deagglomeration of nanoparticle clusters within a few microseconds to even a smaller size than the initial size.

This concept can be integrated to a thermal fluid system with the use of parallel flow restrictive elements embedded to an additional flow component. This addition as a flow component to a system will enable the reusability of nanoparticles in thermal fluid systems and will result in efficiency increase and energy savings.

ACKNOWLEDGMENTS

This study was supported by the TUBITAK (the Scientific and Technological Research Council of Turkey) Support Program for Scientific and Technological Research Project, Grant No. 217M869, and the Sabanci University Internal Project Grant, Grant No. I.A.CF-18-01877. Equipment utilization support from the Sabanci University Nanotechnology Research and Applications Center (SUNUM) is gratefully appreciated.

DATA AVAILABILITY

The data that support the findings of this study are available from the corresponding author upon reasonable request.

REFERENCES

[1] P. P. Gohil and R. P. Saini, "Effect of temperature, suction head and flow velocity on cavitation in a Francis turbine of small hydro power plant," Energy **93**, 613–624 (2015).
[2] L. Albanese, R. Ciriminna, F. Meneguzzo, and M. Pagliaro, "Beer-brewing powered by controlled hydrodynamic cavitation: Theory and real-scale experiments," J. Clean. Prod. **142**, 1457–1470 (2017).
[3] S. Pathania, Q. T. Ho, S. A. Hogan, N. McCarthy, and J. T. Tobin, "Applications of hydrodynamic cavitation for instant rehydration of high protein milk powders," J. Food Eng. **225**, 18–25 (2018).
[4] B. Schneider, A. Koşar, C.-J. Kuo, C. Mishra, G. S. Cole, R. P. Scaringe, and Y. Peles, "Cavitation enhanced heat transfer in microchannels," J. Heat Transfer **128**, 1293–1301 (2006).
[5] J. Cai, X. Huai, S. Liang, and X. Li, "Augmentation of natural convective heat transfer by acoustic cavitation," Front. Energy Power Eng. China **4**, 313–318 (2010).
[6] M. Ghorbani, C. Sozer, G. Alcan, M. Unel, S. Ekici, H. Uvet, and A. Koşar, "Biomedical device prototype based on small scale hydrodynamic cavitation," AIP Adv. **8**, 035108 (2018).
[7] M. T. Gevari, M. Ghorbani, A. J. Svagan, D. Grishenkov, and A. Kosar, "Energy harvesting with micro scale hydrodynamic cavitation-thermoelectric generation coupling," AIP Adv. **9**, 105012 (2019).
[8] M. Ghorbani, A. Mohammadi, A. R. Motezakker, L. G. Villanueva, Y. Leblebici, and A. Koşar, "Energy harvesting in microscale with cavitating flows," ACS Omega **2**, 6870–6877 (2017).
[9] M. Dular, T. Griessler-Bulc, I. Gutierrez-Aguirre, E. Heath, T. Kosjek, A. Krivograd Klemenčič, M. Oder, M. Petkovšek, N. Rački, and M. Ravnikar, A. Šarc, B. Širok, M. Zupanc, M. Žitnik, and B. Kompare, "Use of hydrodynamic cavitation in (waste) water treatment," Ultrason. Sonochem. **29**, 577–588 (2016).
[10] A. Gholami, A. Hajinezhad, F. Pourfayaz, and M. H. Ahmadi, "The effect of hydrodynamic and ultrasonic cavitation on biodiesel production: An exergy analysis approach," Energy **160**, 478–489 (2018).
[11] M. T. Gevari, A. Parlar, M. Torabfam, A. Koşar, M. Yüce, and M. Ghorbani, "Influence of fluid properties on intensity of hydrodynamic cavitation and deactivation of Salmonella typhimurium," Process **8**, 326 (2020).
[12] D. J. Flannigan and K. S. Suslick, "Plasma formation and temperature measurement during single-bubble cavitation," Nature **434**, 52 (2005).
[13] A. Šarc, T. Stepišnik-Perdih, M. Petkovšek, and M. Dular, "The issue of cavitation number value in studies of water treatment by hydrodynamic cavitation," Ultrason. Sonochem. **34**, 51–59 (2017).
[14] K.-S. Im, S.-K. Cheong, C. F. Powell, D. L. Ming-chia, and J. Wang, "Unraveling the geometry dependence of in-nozzle cavitation in high-pressure injectors," Sci. Rep. **3**, 2067 (2013).
[15] M. Ghorbani, A. K. Sadaghiani, L. G. Villanueva, and A. Koşar, "Hydrodynamic cavitation in microfluidic devices with roughened surfaces," J. Micromech. Microeng. **28**, 075016 (2018).
[16] M. Ghorbani, A. S. Aghdam, M. T. Gevari, A. Koşar, F. Ç. Cebeci, D. Grishenkov, and A. J. Svagan, "Facile hydrodynamic cavitation ON CHIP via cellulose nanofibers stabilized perfluorodroplets inside layer-by-layer assembled SLIPS surfaces," Chem. Eng. J. **382**, 122809 (2020).
[17] M. Ghorbani, G. Deprem, E. Ozdemir, A. R. Motezakker, L. G. Villanueva, and A. Koşar, "On 'cavitation on chip' in microfluidic devices with surface and sidewall roughness elements," J. Microelectromech. Syst. **28**, 890–899 (2019).
[18] M. T. Gevari, A. H. Shafaghi, L. G. Villanueva, M. Ghorbani, and A. Kosar, "Engineered lateral roughness element implementation and working fluid alteration to intensify hydrodynamic cavitating flows on a chip for energy harvesting," Micromachines **11**, 49 (2020).
[19] S. Mossaz, D. Colombet, and F. Ayela, "Hydrodynamic cavitation of binary liquid mixtures in laminar and turbulent flow regimes," Exp. Therm. Fluid Sci. **80**, 337–347 (2017).
[20] C. Mishra and Y. Peles, "Development of cavitation in refrigerant (R-123) flow inside rudimentary microfluidic systems," J. Microelectromech. Syst. **15**, 1319–1329 (2006).
[21] M. Ghorbani, H. Chen, L. G. Villanueva, D. Grishenkov, and A. Koşar, "Intensifying cavitating flows in microfluidic devices with poly(vinyl alcohol) (PVA) microbubbles," Phys. Fluids **30**, 102001 (2018).
[22] T. Abbasiasl, S. Niazi, A. S. Aghdam, H. Chen, F. Ç. Cebeci, M. Ghorbani, D. Grishenkov, and A. Koşar, "Effect of intensified cavitation using poly(vinyl alcohol) microbubbles on spray atomization characteristics in microscale," AIP Adv. **10**, 025318 (2020).
[23] P. Ghosh, G. Han, M. De, C. Kim, and V. Rotello, "Gold nanoparticles in delivery applications," Adv. Drug Delivery Rev. **60**, 1307–1315 (2008).
[24] A. D. Sekar, T. Jayabalan, H. Muthukumar, N. I. Chandrasekaran, S. N. Mohamed, and M. Matheswaran, "Enhancing power generation and treatment of dairy waste water in microbial fuel cell using Cu-doped iron oxide nanoparticles decorated anode," Energy **172**, 173–180 (2019).
[25] M. Ghassemi and A. Shahidian, *Nano and Bio Heat Transfer and Fluid Flow* (Academic Press, 2017).
[26] H. Abdolahi-Mansoorkhani and S. Seddighi, "H_2S and CO_2 capture from gaseous fuels using nanoparticle membrane," Energy **168**, 847–857 (2019).
[27] H. S. Huang and J. F. Hainfeld, "Intravenous magnetic nanoparticle cancer hyperthermia," Int. J. Nanomed. **8**, 2521 (2013).
[28] H. Jin, G. Lin, A. Zeiny, L. Bai, and D. Wen, "Nanoparticle-based solar vapor generation: An experimental and numerical study," Energy **178**, 447–459 (2019).
[29] S. U. S. Choi and J. A. Eastman, *Enhancing Thermal Conductivity of Fluids with Nanoparticles* (Argonne National Laboratory, IL, USA, 1995).

© Author(s) 2020

[30]J. M. Mahdi and E. C. Nsofor, "Solidification enhancement in a triplex-tube latent heat energy storage system using nanoparticles-metal foam combination," Energy **126**, 501–512 (2017).
[31]L. Godson, B. Raja, D. Mohan Lal, and S. Wongwises, "Enhancement of heat transfer using nanofluids—An overview," Renewable Sustainable Energy Rev. **14**, 629–641 (2010).
[32]S. Balamurugan and V. Sajith, "Experimental investigation on the stability and abrasive action of cerium oxide nanoparticles dispersed diesel," Energy **131**, 113–124 (2017).
[33]M. Beltrán-Gastélum, M. I. Salazar-Gastélum, J. R. Flores-Hernández, G. G. Botte, S. Pérez-Sicairos, T. Romero-Castañon, E. Reynoso-Soto, and R. M. Félix-Navarro, "Pt-Au nanoparticles on graphene for oxygen reduction reaction: Stability and performance on proton exchange membrane fuel cell," Energy **181**, 1225–1234 (2019).
[34]G. Xia, H. Jiang, R. Liu, and Y. Zhai, "Effects of surfactant on the stability and thermal conductivity of Al_2O_3/de-ionized water nanofluids," Int. J. Therm. Sci. **84**, 118–124 (2014).
[35]W. Yu and H. Xie, "A review on nanofluids: Preparation, stability mechanisms, and applications," J. Nanomater. **2012**, 435873.
[36]X. Yang and Z.-h. Liu, "A kind of nanofluid consisting of surface-functionalized nanoparticles," Nanoscale Res. Lett. **5**, 1324 (2010).
[37]M. T. Gevari, T. Abbasiasl, S. Niazi, M. Ghorbani, and A. Koşar, "Direct and indirect thermal applications of hydrodynamic and acoustic cavitation: A review," Appl. Therm. Eng. **171**, 115065 (2020).
[38]M. Karimzadehkhouei, M. Ghorbani, M. Sezen, K. Şendur, M. Pınar Mengüç, Y. Leblebici, and A. Koşar, "Increasing the stability of nanofluids with cavitating flows in micro orifices," Appl. Phys. Lett. **109**, 104101 (2016).
[39]A. Koşar, K. Şendur, M. P. Mengüç, "Flow system for avoiding particle agglomeration," Patent Application No. PCT/TR2015/050145, 2015.
[40]J. R. DeVore, "Refractive indices of rutile and sphalerite," J. Opt. Soc. Am. **41**, 416–419 (1951).
[41]E. Brennen, *Cavitation and Bubble Dynamics Christopher* (California Institute of Technology, Pasadena, CA, 1995).
[42]M. Ghorbani, A. K. Sadaghiani, M. Yidiz, and A. Koşar, "Experimental and numerical investigations on spray structure under the effect of cavitation phenomenon in a microchannel," J. Mech. Sci. Technol. **31**, 235–247 (2017).
[43]B. Ward and D. C. Emmony, "The energies and pressures of acoustic transients associated with optical cavitation in water," J. Mod. Opt. **37**, 803–811 (1990).

© Author(s) 2020